Thermoelectric properties of transition metals-doped $Ca_3Co_{3.8}M_{0.2}O_{9+\delta}$ (M = Co, Cr, Fe, Ni, Cu and Zn)

ARTICLE *in* JOURNAL OF MATERIALS SCIENCE MATERIALS IN ELECTRONICS · MAY 2011

Impact Factor: 1.57 · DOI: 10.1007/s10854-011-0546-z

4 AUTHORS, INCLUDING:

Supree Pinitsoontorn
Khon Kaen University
50 PUBLICATIONS **297** CITATIONS
SEE PROFILE

N. Keawprak
Thailand Institute of Scientific and Technol…
5 PUBLICATIONS **95** CITATIONS
SEE PROFILE

Vittaya Amornkitbamrung
Khon Kaen University
90 PUBLICATIONS **681** CITATIONS
SEE PROFILE

J Mater Sci: Mater Electron (2012) 23:1050–1056
DOI 10.1007/s10854-011-0546-z

Thermoelectric properties of transition metals-doped $Ca_3Co_{3.8}M_{0.2}O_{9+\delta}$ (M = Co, Cr, Fe, Ni, Cu and Zn)

S. Pinitsoontorn · N. Lerssongkram · N. Keawprak · V. Amornkitbamrung

Received: 8 July 2011 / Accepted: 10 October 2011 / Published online: 20 October 2011

Abstract The thermoelectric properties of the $Ca_3Co_4O_{9+\delta}$ and the transition metals-doped $Ca_3Co_{3.8}M_{0.2}O_{9+\delta}$ (where M = Cr, Fe, Ni, Cu and Zn) ceramics were reported. $Ca_3Co_4O_{9+\delta}$ single phase was checked by using X-ray diffraction analysis performed for the $Ca_3Co_{3.8}M_{0.2}O_{9+\delta}$ samples. The scanning electron micrographs showed some degrees of grains alignment in the compacted direction. The resistivity of the samples measured from 100 up to 700 °C varies in magnitude for different transition metals substitution. The variation of resistivity was explained by a change of carrier concentration induced by the doped ions. The thermopower increased with increasing temperature but showed no obvious change for any transition metals doping. The thermal conductivities changed for the doped samples but were relatively independent of temperature. The *ZT* was calculated to be the highest for the Fe substitution for the whole measurement temperature with the maximum value of 0.12 at 700 °C.

1 Introduction

Thermoelectric modules have a potential for generating power from any source of waste heat. A module consists of a number of interconnecting n-type and p-type thermoelectric materials to produce output power. A good thermoelectric material must be a good electrical conductor, a good thermal insulator and must have a high thermopower, since the energy conversion efficiency of any particular material is defined by its dimensionless figure-of-merit, $ZT = S^2T/\rho\kappa$, where S is the Seebeck coefficient, ρ the electrical resistivity and κ the thermal conductivity. For any real practical use in power generator, the *ZT* should be higher than 1 [1].

Thermoelectric materials are conventionally made of metallic compounds such as Bi_2Te_3 or PbTe [1], due to their good efficiency at room temperature. However, such compounds are not reliable and chemically instable at high temperature. In general, oxides materials are chemically stable at high temperature and, thus, can be used at the temperature of several hundred °C [2]. $Ca_3Co_4O_{9+\delta}$ is one of the potential candidates for thermoelectric applications due to its interesting *ZT* close to 1 in a form of single crystals [3] or thin films [4]. Such performances are believed to be a result of $Ca_3Co_4O_{9+\delta}$ crystallographic structure, consisting of two misfit layers: the CaO–CoO–CaO rocksalt-type layer and the CdI_2-type CoO_2 layer [5]. $Ca_3Co_4O_{9+\delta}$ polycrystals, on the other hand, still exhibits lower performances, with $ZT < 0.3$ [6–10]. This has to be improved before it can be implemented for any real applications.

One way to improve the thermoelectric properties of the polycrystalline $Ca_3Co_4O_{9+\delta}$ is to partially substitute some elements into $Ca_3Co_4O_{9+\delta}$ in order to reduce the electrical resistivity and the thermal conductivity, and to improve the thermopower simultaneously. The substitution can take place either at the Ca-site or at the Co-site. There have been a number of reports on partially substituted elements at Ca-site, for instance, Na [11–14], Y [8], Ag [15–18], Bi [12, 19], Ba [18], Nd [14], Gd [20], Yb [21], and other rare

S. Pinitsoontorn (✉) · N. Lerssongkram · V. Amornkitbamrung
Department of Physics, Faculty of Science, Khon Kaen University, Khon Kaen 40002, Thailand
e-mail: psupree@kku.ac.th

N. Keawprak
Thailand Institute of Scientific and Technological Research, 35 Mu 3 Tambon Khlong Ha, Amphoe Khlong Luang, Pathum Thani 12120, Thailand

earth elements [22–24]. The effect of partial substitution at the Ca-site is mainly to change the charge carrier concentration which results in a change in resistivity. However, elemental doping at the Co-site may have more influential effect on thermoelectric properties since the charge carrier transport of $Ca_3Co_4O_{9+\delta}$ is restricted mostly to the CdI_2-type CoO_2 layer [25], and also the Fermi level lies at the top of the valence band of the CoO_2 [26]. There have been a few experimental studies on partial substitution at the Co-site [6, 9, 24, 27–32], but very few studies reported a complete set of thermoelectric properties (resistivity, thermopower, and thermal conductivity) and the figure-of-merit at high temperature [9, 24, 30]. Thus, in this paper, following our previous work on synthesis, mechanical and magnetic properties [33], we focused on the thermoelectric properties of $Ca_3Co_{4-x}M_xO_{9+\delta}$ (where M is Cr, Fe, Ni, Zn, and Cu). The concentration of the doped transition metals was maintained at $x = 0.2$ to study the effect of different elemental substitution on the thermoelectric properties. The effects of the partial substituted transition metals on the resistivity, thermopower and thermal conductivity were discussed.

2 Experimental details

Nitrate salts of calcium, cobalt, chromium, iron, nickel, and zinc, and the CuO powders were used as a starting materials in the sol–gel synthesis of the $Ca_3Co_4O_{9+\delta}$ (CCO349) and $Ca_3Co_{3.8}M_{0.2}O_{9+\delta}$ (CCO–M) powders, where M = Cr, Fe, Ni, Cu, Zn. The starting batch were mixed in the stoichiometric ratio and dissolved in the citric acid solution. Polyvinyl alcohol (PVA) was added as a dispersant agent. The solution were then heated at 80–100 °C and subsequently calcined at 800 °C for 4 h in air to obtain powders. The powders were ground, uniaxially compacted at 400 MPa to form pellets and then sintered at 890 °C for 4 h in air. The sample densities were about 70–80% of the theoretical density. The pore volume fraction of the undoped sample was 31.2% while those of the samples doped with Cr, Fe, Ni, Cu, Zn were 26.5, 24.6, 25.9, 19.7 and 26.5%, respectively.

The bulk samples were investigated using the X-ray diffraction (XRD) analysis to verify the phase identification by using the XRD diffractometer with Cu-Kα radiation. Morphology of the samples was characterized using a scanning electron microscope (SEM). The powder samples were investigated under an ultraviolet–visible (UV–Vis) spectroscopy to obtain the absorption spectrum. For thermoelectric properties, the Seebeck coefficient and the electrical resistivity were simultaneously measured perpendicular to the pressed direction by using ZEM-2, Ulvac-Riko from 100 to 700 °C. The seebeck coefficient was calculated from the measured voltage difference in the temperature gradient while the electrical resistivity was measured by a DC 4 terminal method using Ni electrodes. The thermal conductivity was calculated from the specific heat capacity and the diffusivity measured parallel to the pressed direction using a laser flash method (TC-7000, Ulvac-Riko) from 100 to 700 °C.

3 Results and discussions

The XRD patterns of the CCO349 and all CCO–M samples can be matched with the standard JCPDS card (21-139) of $Ca_9Co_{12}O_{28}$, without any visible peak of a secondary phase, indicating that the single phase of the transition metals-doped CCO–M was formed. The intensities of the (00*l*) peaks for the bulk samples are much stronger compared with the other (*hkl*) peaks, indicating some grain alignments along the (00*l*) plane of the CCO349 and CCO–M pellets.

The cross-section SEM images of the sintered CCO349 and CCO–M samples are shown in Fig. 1. The grain size for all cases can be estimated to be in the range of 1–5 μm. It can be seen from Fig. 1 that sheet-like or plate-like grains are observed in every sample. This suggested some grain alignments along the (00*l*) plane, as reported for the case of the textured CCO349 [34, 35]. The observation is in agreement with the XRD result for the high intensity of the (00*l*) planes. However, as compared to the SEM images of the recently published paper [36], our samples show a much lower degree of texture. The stronger texture in the present samples can be induced by utilizing other sintering conditions, such as hot-pressing [9, 36], spark plasma sintering [37] or thermoforging [34], for an improvement of the thermoelectric properties of CCO349.

The electrical resistivity of the samples is shown in Fig. 2. The resistivity of every sample does not vary significantly throughout the measurement temperature range. The lowest electrical resistivity belongs to the CCO–Cu with $\rho \sim 10$ mΩ cm throughout the measured temperature. From 200 to 400 °C, every sample show a semiconductor type characteristic (a decrease in resistivity with temperature), for which the charge transport process is the hopping of a hole from Co^{4+} to Co^{3+} in these compounds [37]. On the other hand, over 400 °C all samples, except CCO–Cr, exhibit a slight increase in resistivity with temperature, suggesting metal type behaviour; the charge carriers are transported in the valence or conduction band. It is well known that CCO349 is highly anisotropic with a metallic-like behavior in the a–b plane and a semiconducting behavior along the c-axis [5]. Therefore, the observed resistivity curves in Fig. 2 may be contributed from the mixture of these two types of behavior in different

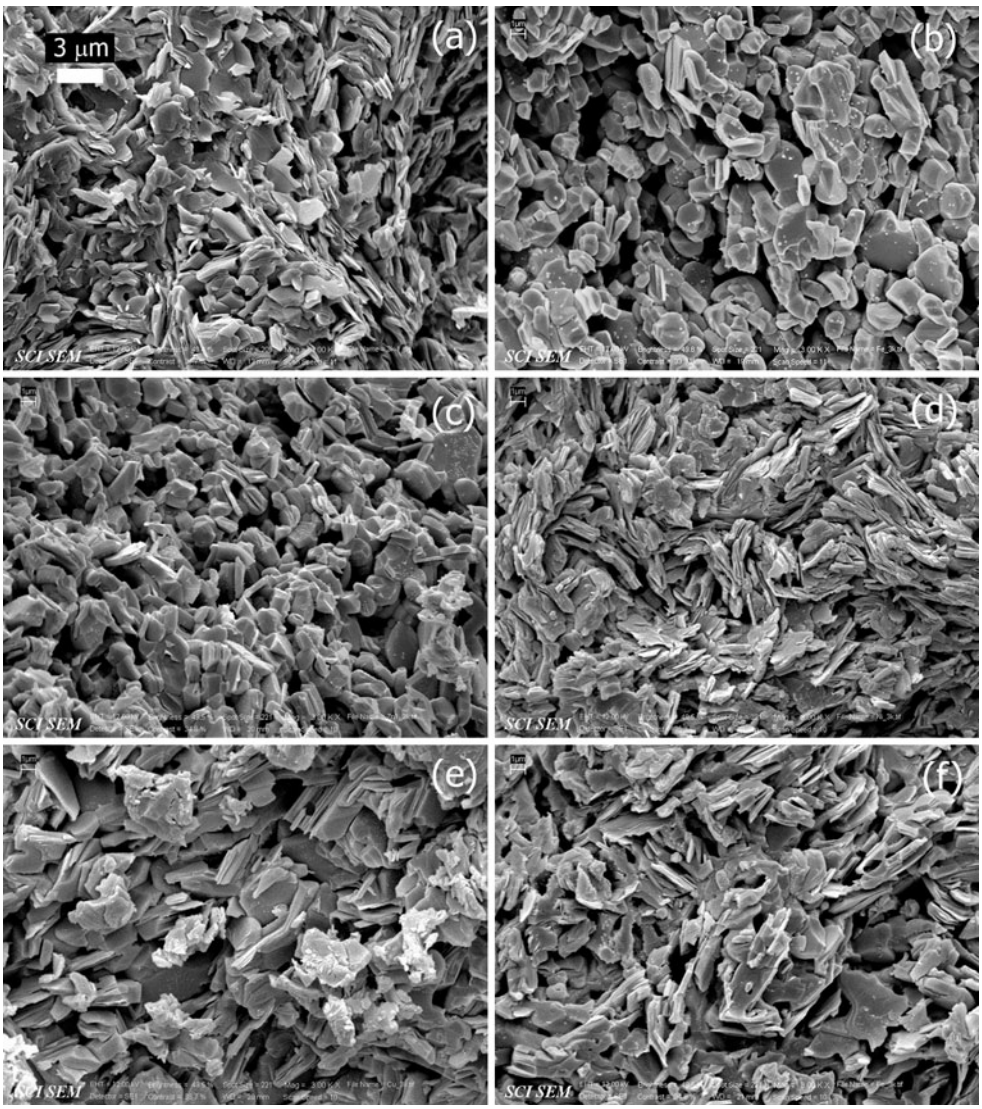

Fig. 1 SEM micrographs of the sintered samples of **a** CCO349, **b** CCO–Cr, **c** CCO–Fe, **d** CCO–Ni, **e** CCO–Cu, **f** CCO–Zn

proportion. The general equation for electrical conductivity (σ) of two carrier types is

$$\sigma = e\left(\mu_p p + \mu_n n\right) \tag{1}$$

where e is the charge of an electron, p the hole concentration, μ_p the mobility of hole, n the electron concentration, and μ_n the mobility of electron. It was found from the Hall measurement that the hole carrier concentration in the polycrystalline doped CCO349 system is in the range of 2–4 $\times$ 10^{20} cm^{-3} [9, 24, 29], and the mobility of hole is $\sim$1.0 cm^2/Vs [24]. Putting in these values into Eq. 1, the electrical conductivity from the hole conduction is approximately 30–60 S/cm, which is in the same order of magnitude with the present measurement. Thus, it can be concluded that the majority carrier is hole and the Eq. 1 can be simplified to a single charge carrier as

$$\sigma = e\mu_p p \tag{2}$$

Compared to the previous results on the single crystal CCO349, the measured resistivity in the present work is about an order of magnitude larger than the single crystal CCO349 [3]. An increase in the resistivity is partly due to a relatively large amount of porosities as seen in the SEM images. However, if we use a simplified Landauer model for the electrical conductivity analysis by assuming zero conductivity of pores, the conductivity of the solid phase can be calculated according to the equation [38]

$$\sigma_m = \sigma_s\left(\frac{3V_f - 1}{2}\right) \tag{3}$$

where σ_m, σ_s and V_f are the measured conductivity, the conductivity of the solid phase, and the volume fraction of the solid phase, respectively. From this model, the

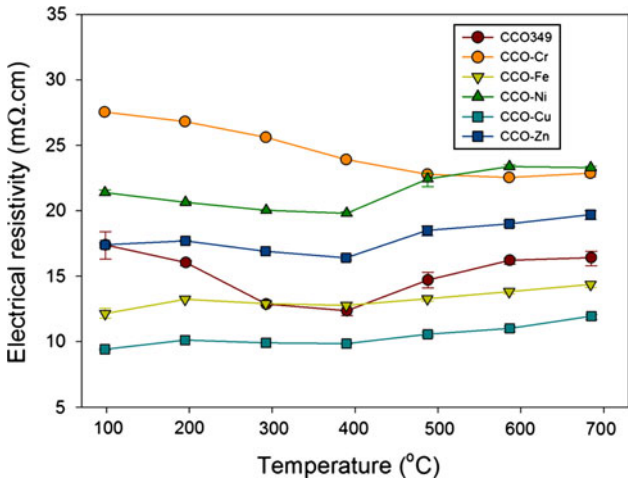

Fig. 2 Temperature dependence of resistivity for CCO349 and CCO–M

resistivity of the CCO phase alone would be roughly halved, which still does not account for an order of magnitude difference with the single crystal. The effect of grain boundaries need to be included since they can scatter charge carrier effectively causing higher resistivity. In addition, Prevel et al. [34] showed that the highly textured polycrystal exhibits much lower resistance (approaching the value for single crystal) than the randomly oriented CCO349. The present samples do not show high degree of texture and that will contribute to a larger electrical resistance.

Substitution of the transition metals for Co does change the magnitude of the resistivity for a maximum of threefold. Partially replacing Co with Fe or Cu reduces the resistivity whereas Cr, Ni and Zn doping results in a higher resistivity. The possible explanations for the observation are as follows. As mentioned prior that the major charge carrier of CCO349 was hole, and assuming the mobility of the carrier does not change significantly by doping, the conductivity is directly proportional to the carrier concentration. Previous studies have shown that the ionic state of the Co ions in the CCO349 structure can be +2, +3 and +4, with the average valence between +3 and +4 [5, 27, 29]. The usual valence states of Fe and Cu ions are Fe^{2+}/Fe^{3+} and Cu^{2+}, respectively [10, 39], which have the lower charge than the average of Co ions. Therefore, partially replacing Co ions with Fe or Cu ions increases the hole concentration, and results in a reduction of the resistivity. The lower resistivity of Cu-doping compared to Fe-doping was accounted for the higher concentration of hole doping. On the other hand, doping Cr at the Co site, increases the resistivity. Consider the common valence state of Cr ion, it can be +2, +3, and +4 [39]. If it is Cr^{2+} or Cr^{3+} substituted for Co ions, it should result in a decrease in the resistivity in the similar manner as in the case for Fe or Cu substitution. The opposite effect was observed, hence, we are inclined to believe that Cr^{4+} should be dominant, which would result in a reduction in hole concentration, and higher resistivity. The effect for Zn or Ni substitution on the change in resistivity is more complicated to be explained. In the case of Zn, the only allowed valence state is Zn^{2+} [39, 40]. Then, Zn doping should enhance the hole concentration of the system and result in the lower resistivity. The contrary was observed and can be explained if we look at the location of the Co-site for the Zn substitution. It is well known that there are two Co-sites in the CCO349 structure: the CdI_2-type layer [CoO_2], and the rocksalt-like structure [Ca_2CoO_3] [5]. The Co cation in the CoO_2 layers are the mixture of Co^{3+} and Co^{4+} and their ionic radii in six-coordination are 0.545 and 0.53 Å, respectively, whereas the Co cation in the rocksalt structure is Co^{2+} with the ionic radius in six-coordination of 0.745 Å [24]. The six-coordinated ionic radius of Zn^{2+} is 0.74 Å [39] closer to Co^{2+} than Co^{3+}/Co^{4+}. It is, thus, more likely that Zn was substituted at the Co-site in the rocksalt structure. The theoretical study [26] and the recent experimental works [10, 25] showed that the conducting carrier is a contribution from the CoO_2 layer. Therefore, the Zn ions substituted in the rocksalt structure probably do not disturb the carrier concentration of the system. The substitution might instead increase scattering sites and result in a larger resistivity as previously reported [21]. Lastly, for the case of Ni doping, the usual valence state of Ni are +2 and +3, with the ionic radii in six-coordination of 0.69 and 0.56 [39]. Ni^{3+} ions, thus, have the tendency to stay at Co-site in the CoO_2 due to the same ionic size. If that is the case, from the above argument we would expect a reduction in resistivity due to hole doping. On the other hand, if Ni^{2+} is the substitutional cation, the effect of the mismatch of the ionic radii would affect the crystal distortion, produce more scattering sites and result in the larger resistivity, as observed in the present work and similar to the previous report [31].

The plot of the Seebeck coefficient (S) versus the temperature is shown in Fig. 3. The thermopower of every sample increases with the measured temperature. The thermopower is at maximum at 700 °C for all samples with S in the range of 170–200 μV/K. The values observed in the present work are in the same order as the previous studies on other doping at the Co-site for the similar temperature range [9, 21, 24, 31]. The Seebeck coefficients in Fig. 3 appear to be independent of different transition metals doping. This point is different from previous studies where they showed a dependence of the S on elemental substitution [8, 10, 12–14, 17, 18, 20, 22, 24, 26, 30, 41]. However, the previous studies did not show any consistency of the S dependence and different methods were used

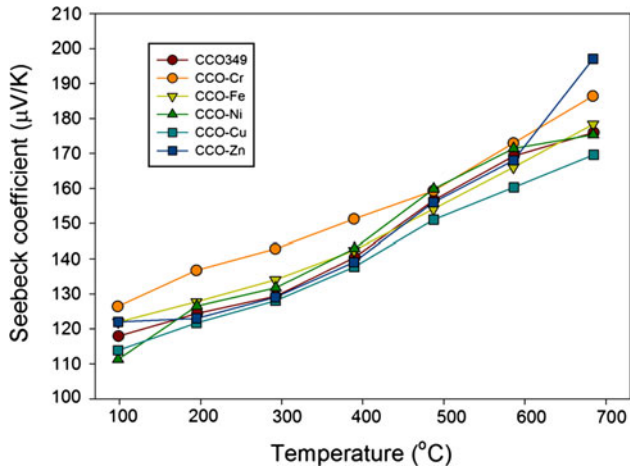

Fig. 3 Temperature dependence of Seebeck coefficient for CCO349 and CCO–M

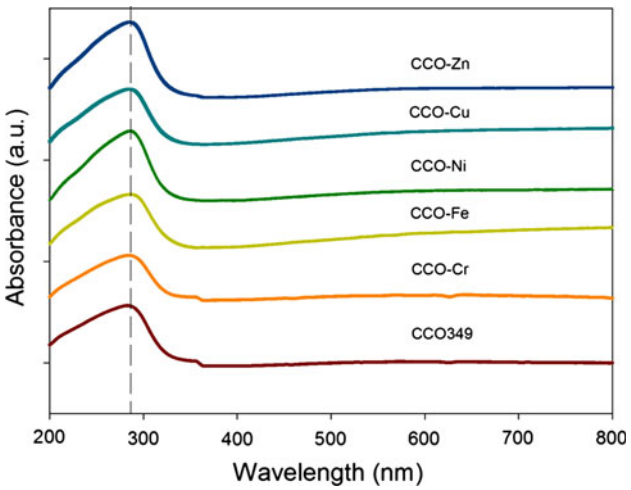

Fig. 4 UV-Vis absorption spectrum for CCO349 and CCO–M

to interpret different results. The first way is to use the model based on the modified Heikes formula [17, 18, 20, 22, 26, 41]

$$S = -\frac{\kappa_B}{e}\left(\ln\frac{g_3}{g_4}\frac{x}{1-x}\right) \tag{4}$$

where g_3 and g_4 are the number of configuration of the Co^{3+} and Co^{4+} ions, respectively, and x the concentration of Co^{4+} ions. With the low spin state of Co^{3+} $\left(t_{2g}^6\right)$ and Co^{4+} $\left(t_{2g}^5\right)$ [27, 28], yielding $g_3 = 1$ and $g_4 = 6$, and the thermopower depends on the fraction of Co^{4+}. On the other hand, some papers chose to explain their results on the basis of the Mott formula [8, 10, 12–14, 24, 30]

$$S = \frac{c_e}{n} + \frac{\pi^2 k_B^2 T}{3e}\left[\frac{\partial \ln \mu(\varepsilon)}{\partial \varepsilon}\right]_{\varepsilon=\varepsilon_F} \tag{5}$$

where c_e and $\mu(\varepsilon)$ are electronic specific heat and energy correlated carrier mobility, respectively. If S increases with decreasing n, it was usually interpreted as the predominance of the first term in Eq. 3. If the opposite effect was found, the second term, which is closely related to the electronic structure, was responsible for the dependence of S. The equations above assume that the change in the thermopower is a result of significant modification in the electronic structure of the CCO349, particularly at near the Fermi level. However, in our case, there is no obvious change in the thermopower with different elemental doping. We can infer that the electronic structure near the Fermi level was not disturbed significantly. The UV–Vis absorption spectrums shown in Fig. 4 also provide the evidence of our inference. The absorption peaks of every sample are at the same wavelength of $\sim$284 nm. The peak widths are very similar though the peak intensity may vary slightly. The similarity of the UV–Vis absorption spectrum

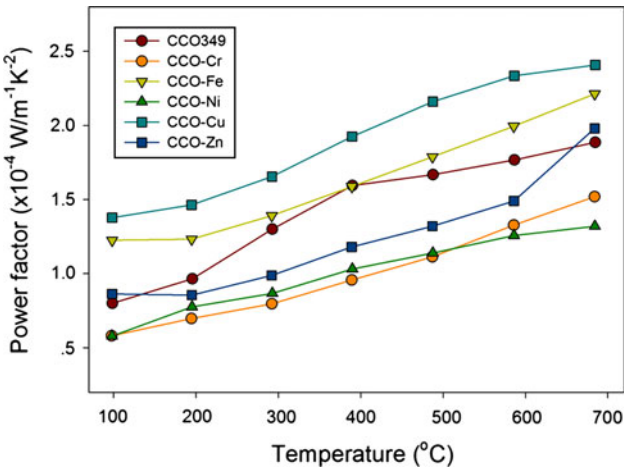

Fig. 5 Temperature dependence of power factor for CCO349 and CCO–M

implies that the electronic structure near the Fermi level of all samples is not significantly different.

Combining the electrical resistivity and the Seebeck coefficient, one can calculate the power factor (S^2/ρ) as shown in Fig. 5. Due to the insignificant variation of the resistivity with temperature, the power factor, thus, follows the same trend of the thermopower. The highest power factor belongs to CCO–Cu for the whole measurement temperature, and has the maximum value of $\sim 2.4 \times 10^{-4}$ W/mK^2 at 700 °C.

The measured thermal conductivities are shown in Fig. 6. Increasing temperature does not show much influential effect on the thermal conductivity. The undoped CCO349 has the thermal conductivity of $\sim$2.5 W/m/K for most measurement temperature, which is the same order of magnitude as the published data [8, 30]. In general, the total thermal conductivity (κ) is a result from two

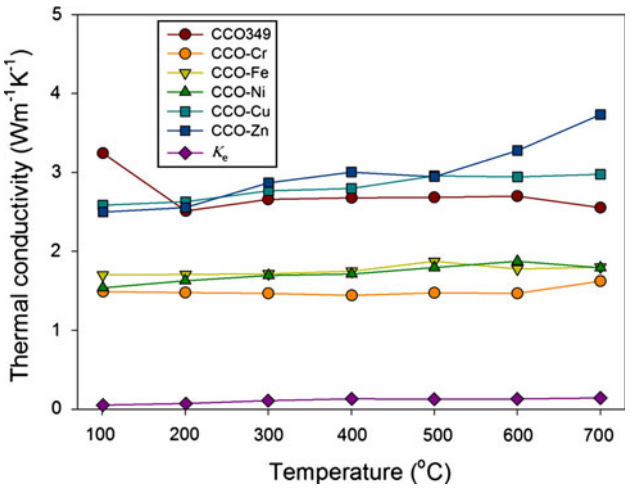

Fig. 6 Temperature dependence of thermal conductivity for CCO349 and CCO–M

contributions: the lattice thermal conductivity (κ_l) and the electronic thermal conductivity (κ_e)according to the equation

$$\kappa = \kappa_l + \kappa_e \tag{6}$$

From the Wiedemann–Franz's law, κ_e is related to the electrical conductivity by the equation

$$\kappa_e = L\sigma T \tag{7}$$

where L is Lorenz factor, 2.44×10^{-8} $W\Omega K^{-2}$. Temperature dependence κ_e of CCO349 is also plotted in Fig. 6. The magnitudes of κ_e for other samples are nearly the same. It can be seen obviously from Fig. 6 that the electronic thermal conductivity does not have much influence on the total conductivity, and the main contribution must come from the lattice vibration. Usually, by substituting other elements to a lattice causes a distortion which would lead to a larger phonon scattering, i.e. smaller κ_l. The result in Fig. 6 will be more pronounced if we consider the effect of porosity and use the simplified Maxwell-Eucken model to calculate thermal conductivity of the solid phase (by assuming zero thermal conductivity of pores) according to the equation [42]

$$\kappa_m = \kappa_s\left(\frac{1 - V_p}{1 + V_p/2}\right) \tag{8}$$

where κ_m, κ_s and V_p are the measured thermal conductivity, the thermal conductivity of the solid phase, and the pore volume fraction, respectively. Putting the pore volume fraction in this model, the thermal conductivities of the solid phase in all doped samples are lower than the undoped one. This, hence, supports the idea of lattice distortion by substituting other elements. However, porosity cannot explain the difference in thermal conductivity for the doped samples since there is no correlation between thermal conductivity and pore volume fractions. Other effects such as texture or defects should be considered. From Fig. 6 it can be seen that doping Cu and Zn raised the thermal conductivity but doping Cr, Fe and Ni showed a decrease. The SEM micrographs in Fig. 1 show that the grain shape for CCO–Cr and CCO–Fe is less plate-like (lower texture) compared to other samples. It was found that a larger number of plate-like grains (higher texture) exhibit higher thermal conductivity than the random shape grains [43]; thus, the reduced thermal conductivity in CCO–Cr and CCO–Fe is possibly contributed from the texture effect. In addition, the thermal conductivity of every sample shows nearly a temperature independent behaviour. The absence of a decrease in thermal conductivity with temperature implies that lattice disorder (defects) has a strong effect compared to phonon—phonon interactions; and thus the defects in samples may be the main contribution to the difference in thermal conductivity of the doped samples.

Figure 7 shows the temperature dependence of the dimensionless figure-of-merit ZT. Although the power factor was the highest for CCO–Cu, its large thermal conductivity contributed to the reduction in ZT, according to $ZT = S^2T/\rho\kappa$. On the other hand, CCO–Fe showed a combination of the relatively high power factor and the low thermal conductivity, resulting in the highest ZT for the whole temperature range for the CCO–M series. The ZT of CCO–Fe at 700 °C is ~0.12 which is approximately 70% higher than the CCO349 at the same temperature. It may be noted that the ZT in the present work is lower than some reported data [9, 24, 30], but the sintering methods were different. Most papers reported on the hot-press or the spark plasma sintering methods used to obtain a very dense sample [8, 9]. Thus, by optimizing the sintering methods, the ZT in the present work can be larger.

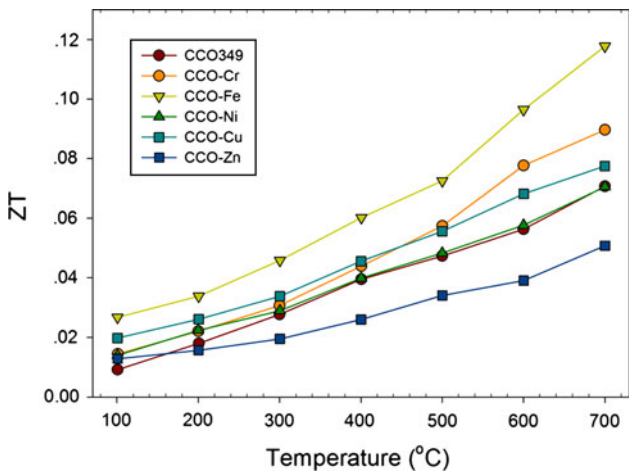

Fig. 7 Temperature dependence of ZT for CCO349 and CCO–M

4 Conclusions

The $Ca_3Co_4O_{9+\delta}$ and the transition metals-doped $Ca_3Co_{3.8}M_{0.2}O_{9+\delta}$ series (where M = Cr, Fe, Ni, Cu and Zn) were successfully synthesized by using a sol–gel method using PVA as a dispersing agent. Some grains alignment along the c-axis was observed from the SEM images, as a result of the uniaxial pressure. Doping transition metals at the Co-site showed an interesting effect on the resistivity, which was explained by the charge and radius of the doped ions. The thermopower, on the other hand, showed no obvious change with doping. This might suggest no significant change of the electronic structure as can be seen from the similar position of the UV–Vis absorption peaks. Partial substitution also played an important role in a change in the thermal conductivities. The sample with partial Fe substitution showed the highest *ZT* of 0.12 at 700 °C, and can be improved by optimizing the sintering method.

Acknowledgments This project was financially supported by Thailand Center of Excellence in Physics, CHE, Ministry of Education, Bangkok 10400, Thailand, and Thailand Research Fund in cooperation with the Commission on Higher Education (Grant No. MRG5380060).

References

1. T.M. Tritt, M.A. Subramanian, MRS Bull. **31**, 188 (2006)
2. K. Koumoto, I. Terasaki, R. Funahashi, MRS Bull. **31**, 206 (2006)
3. M. Shikano, R. Funahashi, Appl. Phys. Lett. **82**, 1851 (2003)
4. H. Ohta, K. Sugiura, K. Koumoto, Inorg. Chem. **47**, 8429 (2008)
5. A.C. Masset, C. Michel, A. Maignan, M. Hervieu, O. Toulemonde, F. Studer, B. Raveau, Phys. Rev. B **62**, 166 (2000)
6. D. Li, X.Y. Qin, Y.J. Gu, J. Zhang, Solid State Commun. **134**, 235 (2005)
7. S. Li, R. Funahashi, I. Matsubara, H. Yamada, K. Ueno, S. Sodeoka, Ceram. Int. **27**, 321 (2001)
8. H.Q. Liu, Y. Song, S.N. Zhang, X.B. Zhao, F.R. Wang, J. Phys. Chem. Solids **70**, 600 (2009)
9. N.V. Nong, C.-J. Liu, M. Ohtaki, J. Alloys Compd. **491**, 53 (2010)
10. Y. Wang, Y. Sui, P. Ren, L. Wang, X.J. Wang, W.H. Su, H.J. Fan, Chem. Mater. **22**, 1155 (2010)
11. J. Nan, J. Wu, Y. Deng, C.W. Nan, J. Eur. Ceram. Soc. **23**, 859 (2003)
12. G.J. Xu, R. Funahashi, M. Shikano, I. Matsubara, Y.Q. Zhou, Appl. Phys. Lett. **80**, 3760 (2002)
13. G.J. Xu, R. Funahashi, M. Shikano, Q.R. Pu, B. Liu, Solid State Commun. **124**, 73 (2002)
14. J. Pei, G. Chen, D.Q. Lu, P.S. Liu, N. Zhou, Solid State Commun. **146**, 283 (2008)
15. Y. Wang, Y. Sui, J. Cheng, X.J. Wang, J.P. Miao, Z.G. Liu, Z.N. Qian, W.H. Su, J. Alloys Compd. **448**, 1 (2008)
16. Y. Wang, Y. Sui, J.G. Cheng, X.J. Wang, W.H. Su, J. Alloys Compd. **477**, 817 (2009)
17. F.P. Zhang, Q.M. Lu, J.X. Zhang, X. Zhang, J. Alloys Compd. **477**, 543 (2009)
18. F.P. Zhang, Q.M. Lu, J.X. Zhang, J. Alloys Compd. **484**, 550 (2009)
19. Y. Song, Q. Sun, L.R. Zhao, F.P. Wang, Z.H. Jiang, Mater. Chem. Phys. **113**, 645 (2009)
20. H.Q. Liu, X.B. Zhao, F. Liu, Y. Song, Q. Sun, T.J. Zhu, F.P. Wang, J. Mater. Sci. **43**, 6933 (2008)
21. J. Xu, C.P. Wei, K. Jia, J. Alloys Compd. **500**, 227 (2010)
22. N.V. Nong, C.J. Liu, M. Ohtaki, J. Alloys Compd. **509**, 977 (2011)
23. M. Prevel, O. Perez, J.G. Noudem, Solid State Sci. **9**, 231 (2007)
24. Y. Wang, Y. Sui, X. Wang, W. Sui, X. Liu, J. Appl. Phys. **107**, 033708 (2010)
25. T. Takeuchi, T. Kondo, T. Takami, H. Takahashi, H. Ikuta, U. Mizutani, K. Soda, R. Funahashi, M. Shikano, M. Mikami, S. Tsuda, T. Yokoya, S. Shin, T. Muro, Phys. Rev. B **69**, 125410 (2004)
26. R. Asahi, J. Sugiyama, T. Tani, Phys. Rev. B **66**, 155103 (2002)
27. J.L. Chen, Y.S. Liu, C.J. Liu, L.C. Huang, C.L. Dong, S.S. Chen, C.L. Chang, J. Phys. D Appl. Phys. **42**, 135418 (2009)
28. C.J. Liu, J.L. Chen, L.C. Huang, Z.R. Lin, C.L. Chang, J. Appl. Phys. **102**, 014908 (2007)
29. C.J. Liu, L.C. Huang, J.S. Wang, Appl. Phys. Lett. **89**, 204102 (2006)
30. L.X. Xu, F. Li, Y. Wang, J. Alloys Compd. **501**, 115 (2010)
31. Q. Yao, D.L. Wang, L.D. Chen, X. Shi, M. Zhou, J. Appl. Phys. **97**, 103905 (2005)
32. Y. Miyazaki, Y. Suzuki, T. Miura, Y. Ono, T. Kajitani, The 22nd international conference on thermoelectrics (2003), p. 203
33. S. Pinitsoontorn, N. Lerssongkram, A. Harnwunggmoung, K. Kurosaki, S. Yamanaka, J. Alloys Compd. **503**, 431 (2010)
34. M. Prevel, S. Lemonnier, Y. Klein, S. Hebert, D. Chateigner, B. Ouladdiaf, J.G. Noudem, J. Appl. Phys. **98**, 093706 (2005)
35. Y.Q. Zhou, I. Matsubara, S. Horii, T. Takeuchi, R. Funahashi, M. Shikano, J. Shimoyama, K. Kishio, W. Shin, N. Izu, N. Murayama, J. Appl. Phys. **93**, 2653 (2003)
36. D. Kenfaui, D. Chateigner, M. Gomina, J.G. Noudem, Int. J. Appl. Ceram. Tech. **8**, 214 (2011)
37. Y.H. Lin, J. Lan, Z.J. Shen, Y.H. Liu, C.W. Nan, J.F. Li, Appl. Phys. Lett. **94**, 072107 (2009)
38. E. Barbier, F. Thevenot, J. Mater. Sci. **27**, 2383 (1992)
39. D.R. Lide, *CRC Handbook of Chemistry and Physics* (CRC Press, Baca Raton, 2003), p. 12
40. I.S. Grigorier, *Handbook of Physical Quantities* (CRC Press, Boca Raton, 1997), p. 44
41. W. Koshibae, K. Tsutsui, S. Maekawa, Phys. Rev. B **62**, 6869 (2000)
42. F.L. Levy, Int. J. Refrig. **4**, 223 (1981)
43. Y. Chen, C. Chen, X. Li, International Conference on Electrical and Control Engineering (2010)